Clustering of particles falling in a turbulent aerosol

K. Gustavsson, S. Vajedi, and B. Mehlig
Department of Physics, Gothenburg University, 41296 Gothenburg, Sweden

Spatial clustering of identical particles falling through a turbulent aerosol enhances the collision rate between the falling particles, an important problem in aerosol science. We analyse this problem using perturbation theory in a dimensionless parameter, the so-called Kubo number. This allows us to derive an analytical theory quantifying the spatial clustering. We find that clustering of small particles in incompressible random velocity fields may be reduced or enhanced by the effect of gravity, depending on the Stokes number of the particles and the Froude number of the flow.

PACS numbers: 05.40.-a,47.55.Kf,47.27.eb

Particles suspended in an incompressible turbulent flow may cluster together even though direct interactions between the particles are negligible. This phenomenon is due to the inertia of the particles. It has been studied extensively in experiments [1–3] (see [4] for a review), in direct numerical simulations (DNS) [5–8], model simulations [9], and by theoretical approaches [10–14]. In most DNS, model simulations, and theoretical studies of clustering, the effect of gravity is neglected. Those DNS that incorporate gravity tend to show that clustering is weakened when gravity causes the particles to fall through the flow [15–19]. But it has also been reported that gravity may increase clustering of particles falling through a turbulent flow [19], see also [15].

Clustering is commonly explained to be due the fact that inertia allows the suspended particles to spiral out from vortices and gather in straining regions of the flow ('Maxey centrifuge effect' [10]). This mechanism was derived assuming that the inertia of the particles is not too large, their Stokes number $\mathrm{St} \equiv 1/(\gamma\tau)$ must be small. Here γ is the Stokes drag coefficient and τ is the smallest characteristic time scale of the flow (the Kolmogorov time in turbulent flows). Even though the fluid-velocity field is incompressible, the particle-velocity field acquires a degree of compressibility due to this effect. The strength of spatial clustering is determined by this divergence. Since the explicit dependence upon the gravitational acceleration $\boldsymbol{g}$ drops out when this divergence is taken, it is argued that gravity does not affect clustering when St is small.

But gravity affects the fluctuations of the flow-velocity gradients seen by the falling particles. In particular, if the fluid Froude number $\mathrm{Fr} \equiv |\boldsymbol{g}|\tau/u_0$ is large enough (u_0 is the Kolmogorov speed), then gravity pulls the particles through the vortices. Do the particles have time to spiral out from the vortices, or is the Maxey effect destroyed? What happens at larger St where 'preferential sampling' in the absence of gravity is strong, but the particle positions are less correlated with the straining regions of the flow? Which effect does gravity have in this case? What is the effect of the anisotropy in the spatial patterns introduced by gravity (Fig. 1)?

Particles may cluster at stagnation points of the flow. This effect is weak in incompressible flows, but may be large in compressible flows where stagnation points occur close to sinks of the flow [20]. How is the clustering at stagnation points modified by gravity? It has been argued that particles are trapped in regions where the settling velocity is compensated by the fluid velocity $\boldsymbol{u}$ of large eddies [21]. Is there clustering at the corresponding stagnation points?

Finally, the inertial particle dynamics exhibits 'caustics' [22, 23] where the phase-space manifold folds over that describes the position dependence of the particle velocities. This gives rise to large velocity differences between close-by particles [24–29]. How is the rate of caustic formation affected by gravity?

In order to answer these questions and to quantify the degree of clustering of particles falling through a turbulent flow we analyse a model system: particles subject to gravity in a random velocity field in two spatial dimensions (see [14] and caption of Fig. 1). We expect no essential difference in three dimensions. The model has three dimensionless parameters: St, Fr, and Ku. The Kubo number $\mathrm{Ku} \equiv u_0\tau/\eta$ (η is the smallest characteristic length scale of the flow) is a dimensionless correlation time. For general values of Fr and St we compute the dynamics of the falling particles perturbatively, taking into account recursively that the perturbations due to the flow velocity cause the actual particle trajectory to deviate from its deterministic path. This yields an expansion in Ku [14, 30, 31], and results in analytical expressions for the clustering as a function of St, Fr, and Ku.

Neglecting effects due to finite particle size, we model the dynamics of a particle as

$$\dot{\boldsymbol{r}} = \mathrm{Ku}\,\boldsymbol{v}\,, \qquad \dot{\boldsymbol{v}} = (\boldsymbol{u}(\boldsymbol{r},t) - \boldsymbol{v})/\,\mathrm{St} + \mathrm{Fr}\,\hat{\boldsymbol{g}}\,. \tag{1}$$

Here dots denote time derivatives, $\boldsymbol{r}$ and $\boldsymbol{v}$ are particle position and velocity, $\boldsymbol{u}(\boldsymbol{r},t)$ is the fluid velocity evaluated at the particle position, and $\hat{\boldsymbol{g}} \equiv \boldsymbol{g}/|\boldsymbol{g}|$ is taken to point in the negative y-direction. Note that gravity does not affect advected particles ($\mathrm{St} \to 0$). In Eq. (1) time- space- and speed scales are dedimensionalised by the characteristic scales τ, η, and u_0 of the flow.

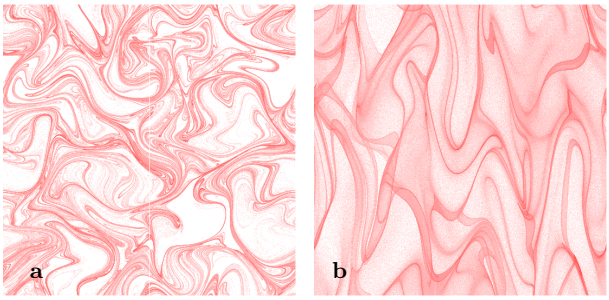

FIG. 1: *(Online colour).* Density of particles falling in a two-dimensional random velocity field $\boldsymbol{u}(\boldsymbol{r},t)=\boldsymbol{\nabla}\psi(\boldsymbol{r},t)\wedge\hat{\boldsymbol{e}}_3$ in the negative y-direction according to Eq. (1). Here $\hat{\boldsymbol{e}}_3$ is a unit vector orthogonal to the plane, and ψ is a Gaussian random function with zero mean and $\langle\psi(\boldsymbol{r},t)\psi(\boldsymbol{0},0)\rangle = (u_0^2\eta^2/2)\exp[-|t|/\tau - \boldsymbol{r}^2/(2\eta^2)]$. White/red regions show low/high particle densities. Particles were initially uniformly distributed with velocities equal to the settling velocity $\boldsymbol{v}_{\rm s}$, and were followed for 100τ. Size of the area shown: $10\eta\times10\eta$. Parameters: Ku = 1, Fr = 1, St = 0.2 (**a**) and St = 10 (**b**).

Preferential sampling is characterised by the divergence of the particle-velocity field $\boldsymbol{\nabla}\cdot\boldsymbol{v}$, see Refs. [10, 14]. Following [11, 13, 14] we compute the time average of $\boldsymbol{\nabla}\cdot\boldsymbol{v}$ in terms of the matrix $\mathbb{Z}$ of the particle-velocity gradients, $Z_{ij}\equiv\partial v_i/\partial r_j$. The dynamics of $\mathbb{Z}$ follows from Eq. (1): $\dot{\mathbb{Z}}=\mathrm{St}^{-1}(\mathbb{A}(\boldsymbol{r},t)-\mathbb{Z})-\mathrm{Ku}\,\mathbb{Z}^2$. In this equation, gravity does not appear explicitly. But its effect is implicit in the dynamics of the matrix $\mathbb{A}$ of fluid-velocity gradients with elements $A_{ij}\equiv\partial u_i/\partial r_j$. To compute the dynamics of $\mathbb{A}(\boldsymbol{r}_t,t)$ along a trajectory $\boldsymbol{r}_t$, we expand around the deterministic ($\boldsymbol{u}=\boldsymbol{0}$) solution $\boldsymbol{r}_t^{(\rm d)}$ of Eq. (1):

$$\boldsymbol{r}_t^{(\rm d)}=\boldsymbol{r}_0+\mathrm{Ku}\,\boldsymbol{v}_{\rm s}t-\mathrm{Ku}\,\mathrm{St}(\boldsymbol{v}_0-\boldsymbol{v}_{\rm s})e^{-t/\,\mathrm{St}}\,. \qquad (2)$$

Here $\boldsymbol{v}_{\rm s}\equiv\mathrm{Fr}\,\mathrm{St}\,\hat{\boldsymbol{g}}$ is the settling velocity of Eq. (1) with $\boldsymbol{u}=0$. The deviation $\delta\boldsymbol{r}_t\equiv\boldsymbol{r}_t-\boldsymbol{r}_t^{(\rm d)}$ is given by the implicit solution of Eq. (1):

$$\delta\boldsymbol{r}_t=\frac{\mathrm{Ku}}{\mathrm{St}}\int_0^t\mathrm{d}t_1\int_0^{t_1}\mathrm{d}t_2 e^{(t_2-t_1)/\,\mathrm{St}}\boldsymbol{u}(\boldsymbol{r}_{t_2},t_2)\,. \qquad (3)$$

For small Ku the deviation $\delta\boldsymbol{r}_t$ is small. This allows a perturbation expansion in Ku [14, 30, 31]. But here we expand around $\boldsymbol{r}_t^{(\rm d)}$ instead of $\boldsymbol{r}_0$. We compute the steady-state average $\langle\mathrm{Tr}\,\mathbb{Z}\rangle_\infty=\langle\boldsymbol{\nabla}\cdot\boldsymbol{v}\rangle_\infty$ using the known statistics of $\boldsymbol{u}(\boldsymbol{r},t)$. To order Ku^3 we find

$$\begin{aligned}\langle\boldsymbol{\nabla}\cdot\boldsymbol{v}\rangle_\infty=\frac{3\,\mathrm{Ku}^3}{4\,\mathrm{St}^5\,\mathrm{G}^8}\Big\{&2\,\mathrm{G}^2\,\mathrm{St}^3(5+4\,\mathrm{St}+3\,\mathrm{St}^2-\mathrm{G}^2\,\mathrm{St}^2(1+\mathrm{St}))+(1+\mathrm{St})^3(2(1+\mathrm{St})^2-\mathrm{G}^2\,\mathrm{St}^2(\mathrm{St}-3))\,\mathcal{F}\left[\frac{1+\mathrm{St}}{\sqrt{2}\,\mathrm{St}\,\mathrm{G}}\right]^2\\
&-\sqrt{2}\,\mathrm{G}\,\mathrm{St}^2(13+17\,\mathrm{St}+15\,\mathrm{St}^2+3\,\mathrm{St}^3+\mathrm{G}^2\,\mathrm{St}^2(4-\mathrm{St}-3\,\mathrm{St}^2)+\mathrm{G}^4\,\mathrm{St}^4)\,\mathcal{F}\left[\frac{1+\mathrm{St}}{\sqrt{2}\,\mathrm{St}\,\mathrm{G}}\right]-4\,\mathrm{G}\,\mathrm{St}(1+\mathrm{St}^2(2+\mathrm{St}^2+\mathrm{G}^2))\,\mathcal{F}\left[\frac{1}{\mathrm{G}}\right]\\
&-2\sqrt{\pi}(1+\mathrm{St}^2)\,\mathrm{G}(-2+\mathrm{St}^2(-2+(-3+\mathrm{St}^2)\,\mathrm{G}^2))\int_0^\infty\mathrm{d}t\exp\left[\mathrm{G}^{-2}-t/\mathrm{St}-\mathrm{G}^2\,t^2/4\right]\mathrm{erfc}\left[\mathrm{G}^{-1}+\mathrm{G}\,t/2\right]\Big\}\,, \qquad (4)\end{aligned}$$

where $\mathcal{F}[x]\equiv\sqrt{\pi}e^{x^2}\,\mathrm{erfc}(x)$ and $\mathrm{G}\equiv\mathrm{Ku}\,\mathrm{St}\,\mathrm{Fr}$ (Ku is small but G can take any value). We now discuss the implications of Eq. (4).

Centrifuge effect at small St. A series expansion of Eq. (4) to lowest order in St with G treated as an independent parameter gives :

$$\begin{aligned}\langle\boldsymbol{\nabla}\cdot\boldsymbol{v}\rangle_\infty\sim\,&3\,\mathrm{Ku}^3\,\mathrm{St}^2/(4\,\mathrm{G}^5)\\
&\times(4\,\mathrm{G}-6\,\mathrm{G}^3-(4-4\,\mathrm{G}^2+3\,\mathrm{G}^4)\,\mathcal{F}[\mathrm{G}^{-1}])\,. \qquad (5)\end{aligned}$$

For Fr = 0 the strength of the centrifuge effect is determined by $\langle\boldsymbol{\nabla}\cdot\boldsymbol{v}\rangle_\infty\sim-\mathrm{Ku}\,\mathrm{St}\langle\mathrm{Tr}\,\mathbb{A}^2\rangle_\infty$ [10, 14]. It turns out that the for Fr > 0 rhs of Eq. (5) is still of this form. We have verified this by repeating the expansion leading to Eq. (4) for $\langle\mathrm{Tr}\,\mathbb{A}^2\rangle_\infty$ to lowest order in St. When G is small in Eq. (5) (for small and moderate values of Fr) we find:

$$\langle\boldsymbol{\nabla}\cdot\boldsymbol{v}\rangle_\infty\sim-6\,\mathrm{Ku}^3\,\mathrm{St}^2\,. \qquad (6)$$

This is exactly the result obtained from the Maxey centrifuge effect in the absence of gravity [14]. In this limit gravity does not modify the centrifuge effect.

Preferential concentration at larger values of St. Expanding Eq. (4) for small values of G yields:

$$\begin{aligned}\langle\boldsymbol{\nabla}\cdot\boldsymbol{v}\rangle_\infty=&-6\,\mathrm{Ku}^3\,\mathrm{St}^2\,\frac{1+3\,\mathrm{St}+\mathrm{St}^2}{(1+\mathrm{St})^3} \qquad (7)\\
&+9\,\mathrm{Ku}^3\,\mathrm{G}^2\,\mathrm{St}^2\,\frac{1+5\,\mathrm{St}+12\,\mathrm{St}^2+20\,\mathrm{St}^3+4\,\mathrm{St}^4}{(1+\mathrm{St})^5}+\ldots\,.\end{aligned}$$

Eq. (7) shows that gravity reduces preferential sampling for all values of St provided G and Ku are small. We attribute this reduction to the fact that gravity causes particles to fall through structures in the flow, rendering preferential sampling in incompressible flow structures less efficient. We note, however, that sinks in compressible flows may act as particle traps for falling particles,

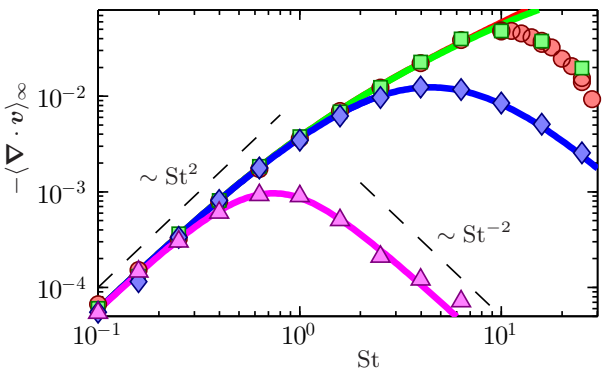

FIG. 2: *(Online colour).* Average divergence of particle velocity field $\langle\boldsymbol{\nabla}\cdot\boldsymbol{v}\rangle_\infty$ shown as a function of St for Ku = 0.1. Markers show data from numerical simulations of Eq. (1). Lines show Eq. (4). Parameters: Fr = 0 (red,○), Fr = 0.1 (green,□), Fr = 1 (blue,◊), Fr = 10 (magenta,△). Black dashed curves show the slopes of the asymptotes (6) and (8).

making preferential sampling more efficient when gravity is present. We have confirmed this observation by generalising Eq. (4) to compressible flows.

Our analytical result (4) is compared to results of numerical simulations of Eq. (1) for Ku = 0.1 in Fig. 2. We observe good agreement except when G is small and St is large.

In the limit of large G and St, Eq. (4) approaches

$$\langle\boldsymbol{\nabla}\cdot\boldsymbol{v}\rangle_\infty \sim -3\sqrt{2\pi}/(4\,\mathrm{Fr}^3\,\mathrm{St}^2)\,. \tag{8}$$

This result matches the Maxey limit (6) at $\mathrm{St}_{\max} \sim (\mathrm{Fr}\,\mathrm{Ku})^{-3/4}$. Our theory shows that gravity decreases $|\langle\boldsymbol{\nabla}\cdot\boldsymbol{v}\rangle_\infty|$ strongly for $\mathrm{St} > \mathrm{St}_{\max}$.

Clustering of rapidly falling particles. Particles with large settling speeds are insensitive to instantaneous fluid configurations. One might expect them to fall uniformly distributed. But Fig. 1**b** shows that rapidly falling particles may cluster. We quantify the degree of clustering by the spatial Lyapunov exponents

$$\lambda_1 \equiv \lim_{t\to\infty} t^{-1}\ln R_t\,, \quad \lambda_1+\lambda_2 \equiv \lim_{t\to\infty} t^{-1}\ln \mathcal{A}_t\,, \tag{9}$$

the expansion (contraction) rates of the spatial separation R_t between two initially nearby particles, and of the area element $\mathcal{A}_t$ spanned by the separation vectors between three nearby particles [9, 11, 13, 32–34]. The Lyapunov exponents characterise the spatial distribution of the particles; they form a fractal with dimension [35]

$$d_\mathrm{L} \equiv 2 - (\lambda_1+\lambda_2)/\lambda_2 \tag{10}$$

(assuming $\lambda_1 > 0$ and $\lambda_1+\lambda_2 < 0$).

We now show how to evaluate Eq. (10) in the limit of rapidly settling particles (Fig. 1**b**), assuming that $\mathrm{G} \gg 1$. The deterministic settling trajectory is $\boldsymbol{r}_t^{(\mathrm{d})} = \mathrm{G}\,t$ (assuming $\boldsymbol{r}_0 = 0$ and $\boldsymbol{v}_0 = \boldsymbol{v}_\mathrm{s}$ in Eq. (2)), and the

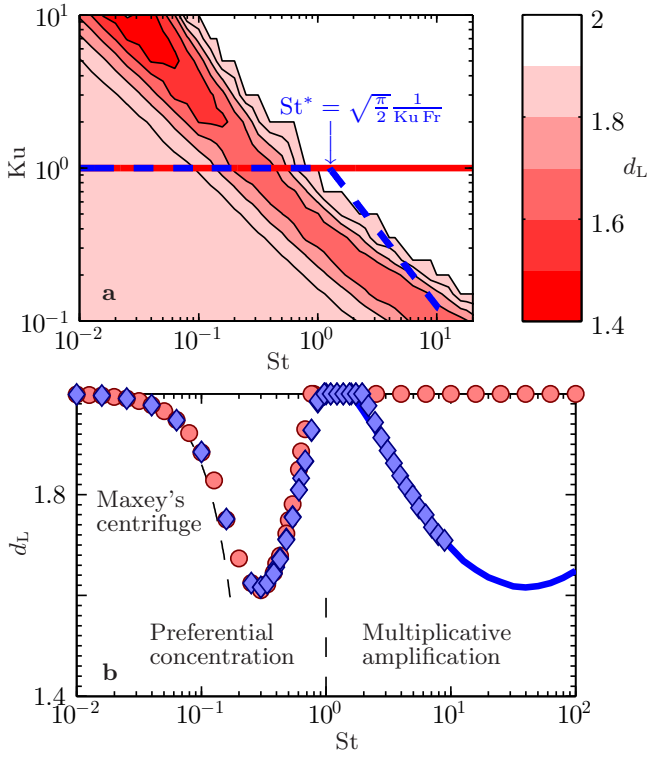

FIG. 3: *(Online colour).* Fractal dimension d_L from numerical simulations of Eq. (1). **a** Contour plot of d_L as a function St and Ku for Fr = 0. Lines show Ku_eff, (13), as a function of St for Fr = 0 (solid red) and for Fr = 1 (dashed blue). For Fr = 1, $\mathrm{St}^* \approx 1.25$. See Eq. (13). **b** Shows d_L versus St with Ku = 1 for Fr = 0 (red,○) and Fr = 1 (green,□). Black dashed line shows limiting behaviour $d_\mathrm{L} \sim 2 - C_\mathrm{Ku}\,\mathrm{St}^2$ (coefficient $C_1 = 14$ was fitted). Blue solid line shows results of numerical integration of Eqs. (11) and (12).

particles experience rapid fluctuations of the flow velocity $\boldsymbol{u}(\boldsymbol{r}_t^{(\mathrm{d})}, t)$. In this limit we approximate the dynamics of the separation $\boldsymbol{R}$ [$R = |\boldsymbol{R}|$ in Eq. (9)] and the relative velocity $\boldsymbol{V}$ between two particles by a Langevin equation:

$$\delta\boldsymbol{R}' = \boldsymbol{V}'\,\delta t'\,, \qquad \delta\boldsymbol{V}' = -\boldsymbol{V}'\,\delta t' + \delta\boldsymbol{F}\,. \tag{11}$$

Here we rescaled $t = t'\,\mathrm{St}$ and $\boldsymbol{v} = \boldsymbol{v}'/(\mathrm{Ku}\,\mathrm{St})$ as convenient in the white-noise limit [11–13, 30]. Further $\delta\boldsymbol{F}$ is Gaussian white noise with zero mean and variance $\langle\delta F_i\delta F_j\rangle = 2\delta t'\,\mathrm{Ku}^2\,\mathrm{St}\sum_{kl} D_{ik,jl}R_kR_l$. The non-zero $D_{ik,jl}$ are given by

$$\begin{aligned} D_{21,21} &= \frac{3}{\sqrt{8}G}\,\mathcal{F}\left[\frac{1}{\sqrt{2}\,\mathrm{G}}\right],\; D_{12,12} = \frac{\mathrm{G}^2-1}{2\,\mathrm{G}^4} + \frac{D_{21,21}}{3\,\mathrm{G}^4}\,,\\ D_{11,11} &= D_{22,22} = -D_{11,22} = -D_{22,11} = -D_{12,21}\\ &= -D_{21,12} = \frac{1}{2\,\mathrm{G}^2} - \frac{D_{21,21}}{3\,\mathrm{G}^2}\,. \end{aligned} \tag{12}$$

Since $D_{12,12} \neq D_{21,21}$ we see that gravity breaks isotropy. This anisotropy is visible in the vertically extended structures in Fig. 1**b**, compared to the more isotropic structures in Fig. 1**a**. In Fig. 3**b** we show d_L obtained by

numerically integrating Eqs. (11) and (12). We observe good agreement with the results of direct numerical simulations of Eq. (1).

A qualitative explanation of the clustering of rapidly falling particles goes as follows. Fig. 3**a** shows the degree of clustering as a function of St and Ku for Fr = 0. For large values of G the diffusion constant $D_{21,21} \sim \mathrm{G}^{-1}$ dominates in Eq. (12). When Fr = 0 the diffusion coefficients in Eq. (12) are independent of Ku and St. We map the Fr > 0 dynamics onto the Fr = 0-dynamics by defining an effective Kubo number, $\mathrm{Ku_{eff}}$, defined so that $D_{21,21}|_{\mathrm{Ku=Ku_{eff}}}$ equals $D_{21,21}|_{\mathrm{Fr=0}}$

$$\mathrm{Ku_{eff}} \sim \begin{cases} \mathrm{Ku} & \text{if } \mathrm{St} \ll \mathrm{St}^* \\ \sqrt{\pi/2}/(\mathrm{Fr\,St}) & \text{if } \mathrm{St} \gg \mathrm{St}^* \end{cases} . \qquad (13)$$

Here $\mathrm{St}^* = \sqrt{\pi/2}/(\mathrm{Ku\,Fr})$ is the scale at which the large G asymptote $D_{21,21} \sim G^{-1}$ meets the G = 0 asymptote.

Following the curve $\mathrm{Ku_{eff}}$ for Ku = 1 shown in Fig. 3**a**, the clustering is approximately unmodified for $\mathrm{St} < \mathrm{St}^*$ [see Fig. 3**b**]. When $\mathrm{St} > \mathrm{St}^*$ the effective Kubo number rapidly becomes so small that the curve reenters the region in parameter space where clustering occurs. In this limit the clustering is caused by many independent random accelerations ('multiplicative amplification') [14], the instantaneous fluid configuration plays no role.

The example Ku = Fr = 1 shown in Fig. 3**a** generalises to other parameter values. Eq. (13) shows that larger values of Ku Fr alter St^* to shift the curve $\mathrm{Ku_{eff}}$ towards smaller values of St. Larger values of Ku shift the curve towards larger $\mathrm{Ku_{eff}}$. In the white-noise limit, clustering is strongest near $\mathrm{Ku} \sim 0.3\,\mathrm{St}^{-1/2}$ (Fig. 1 in [36]). This line is crossed for large enough values of St if $\mathrm{St}^* > 0.1\,\mathrm{Ku}^{-2}$, i.e. if $\mathrm{Fr} < 10\,\mathrm{Ku}$. For larger values of Fr the curve turns early and clustering may be small for all values of St (c.f. Fr = 1 and Fr = 10 in Fig. 2).

Finally, we emphasise that this picture is simplified. When $\boldsymbol{G} < 1$ then the situation is more complicated because the correlation functions sampled by the falling particles are modified. This is reflected in Eq. (4).

Caustics. When caustics are frequent, the expansion leading to Eq. (4) and related expansions in the white-noise limit do not converge, as seen in Fig. 2 for large values of St and Fr = 0), and discussed elsewhere [11, 13, 14]. However, for $\mathrm{St} > \mathrm{St}^*$ caustics are less frequent: in the white-noise limit the rate of caustic formation is of the form $\mathcal{J} \sim e^{-1/(3\,\mathrm{Ku}^2\,\mathrm{St})}$ [22]. It follows from Eq. (13) that $e^{-1/(3\,\mathrm{Ku_{eff}^2\,St})}$ is small in this regime. We thus expect that perturbation theory in $\mathrm{Ku_{eff}}$ could work well in this regime. We note that caustics are rare when St^* is so small that the curve in Fig. 3**a** turns before caustics are activated.

Conclusions. We have derived an analytical theory describing spatial clustering of particles falling through a turbulent aerosol. The theory makes it possible to determine how the clustering depends on the dimensionless parameters of the problem, Fr, St, and Ku.

For small and intermediate values of St, particles falling at finite Fr cluster less, because correlations between particles and flow structures are destroyed. But at very small values of St, unless Fr is very large, clustering due to the Maxey centrifuge effect is only slightly reduced, while clustering at intermediate values of St is reduced more. In compressible flows the situation is entirely different. In this case we find that gravity *enhances* clustering at the stagnation points. This difference may be due the fact that clustering by the centrifuge effect takes longer time [the clustering time scale is $(\lambda_1+\lambda_2)^{-1} \sim \mathrm{St}^{-2}$] and is thus more sensitive to decorrelations than clustering at stagnation points in compressible flows [$(\lambda_1 + \lambda_2)^{-1} \sim$ const.]. But how clustering at stagnation points of $\boldsymbol{u}$ and $\boldsymbol{u} - \boldsymbol{v}_\mathrm{s}$ in incompressible flows is modified by gravity remains an open question.

For large values of St, our calculations show that gravity may increase clustering: if the particles fall rapidly enough, the signal seen by the particles can be approximated by a white-noise model. In this limit we find significant clustering, and the mechanism (multiplicative amplification) is different from that causing clustering at small Stokes numbers. In turbulent flows sweeping by large eddies may affect the dynamics of rapidly falling particles. In [19] it is argued that the clustering of rapidly falling particles is caused by interactions with large eddies. It would be of great interest to compare the strengths of these two mechanisms.

Finally, we find that the rate of caustic formation is reduced when St is large and Fr not too small.

The problem of particles falling under gravity through a turbulent aerosol is important for rain initiation in warm turbulent rain clouds [37]. In this case the Stokes number takes values $\mathrm{St} \sim 10^{-3}(a/\mu\mathrm{m})^2$ [38]. The Stokes number increases four decades as water droplets grow from $\mathrm{St} \sim 10^{-3}$ for small droplets (size 1μm) to St ∼ 10 for large droplets ($100\,\mu$m). In the absence of gravity in a flow with Ku ∼ 1, clustering is largest when St is of order unity. Typical values of the characteristic scales in vigorously turbulent rain clouds are $\tau \sim 10\,\mathrm{ms}$, $\eta \sim 1\,\mathrm{mm}$ and $u_0 \sim 0.1\,\mathrm{m/s}$ [38] which gives Ku and Fr of order unity (blue curve in Fig. 3). Gravity starts to become important for the motion of droplets larger than about $20\,\mu$m [39]. This value (St ∼ 0.4) is consistent with the findings in this Letter. Since gravity mainly affects large particles it is necessary to investigate under which circumstances corrections to the point-particle approximation may become relevant.

In summary our model calculations have shown that the inertial response of the suspended particles to flow fluctuations and the effect of gravity are not additive. They interact in intricate ways giving rise to a rich phase diagram in the dimensionless parameters Ku, St, and Fr.

[1] E.-W. Saw, R. Shaw, S. Ayyalasomayajula, P. Chuang, and A. Gylfason, Phys. Rev. Lett. **100**, 214501 (2008).
[2] J. Salazar, J. de Jonag, L. Cao, S. H. Woodward, H. Meng, and L. Collins, J. Fluid Mech. **600**, 245 (2008).
[3] M. Gibert, H. Xu, and E. Bodenschatz, J. Fluid Mech. **698**, 160 (2012).
[4] Z. Warhaft, Fluid Dyn. Res. **41**, 011201 (2009).
[5] J. Chun, D. L. Koch, S. L. Rani, A. Ahluwalia, and L. R. Collins, J. Fluid Mech. **536**, 219 (2005).
[6] J. Bec, L. Biferale, G. Boffetta, M. Cencini, S. Musacchio, and F. Toschi, Phys. Fluids **18**, 091702 (2006).
[7] E. Calzavarini, M. Cencini, D. Lohse, and F. Toschi, Phys. Rev. Lett. **101**, 084504 (2009).
[8] E. Meneguz and M. Reeks, J. Fluid Mech. **686**, 338 (2010).
[9] J. Bec, Phys. Fluids **15**, 81 (2003).
[10] M. R. Maxey, J. Fluid Mech. **174**, 441 (1987).
[11] K. Duncan, B. Mehlig, S. Östlund, and M. Wilkinson, Phys. Rev. Lett. **95**, 240602 (2005).
[12] B. Mehlig, M. Wilkinson, K. Duncan, T. Weber, and M. Ljunggren, Phys. Rev. E **72**, 051104 (2005).
[13] M. Wilkinson, B. Mehlig, S. Östlund, and K. P. Duncan, Phys. Fluids **19**, 113303(R) (2007).
[14] K. Gustavsson and B. Mehlig, Europhys. Lett. **96**, 60012 (2011).
[15] G. Falkovich and A. Pumir, Phys. Fluids **16**, L47 (2004).
[16] L. Wang, O. Ayala, Y. Xue, and W. Grabowski, J. Atmos. Sci. **63**, 2397 (2006).
[17] C. Franklin, P. Vaillancourt, and M. Yau, J. Atmos. Sci. **64**, 938 (2007).
[18] O. Ayala, B. Rosa, L.-P. Wang, and W. Grabowski, New J. Phys. **10**, 075015 (2008).
[19] E. Woittiez, H. Jonker, and L. Portela, J. Atmos. Sci. **66**, 1926 (2009).
[20] K. Gustavsson and B. Mehlig, J. Stat. Phys. **153**, 813 (2013).
[21] M. Pinsky and A. Khain, Q. J. R. Meteorol. Soc. **123**, 165 (1997).
[22] M. Wilkinson, B. Mehlig, and V. Bezuglyy, Europhys. Lett. **71**, 186 (2005).
[23] M. Wilkinson, B. Mehlig, and V. Bezuglyy, Phys. Rev. Lett. **97**, 048501 (2006).
[24] G. Falkovich, A. Fouxon, and G. Stepanov, Nature **419**, 151 (2002).
[25] J. Bec, L. Biferale, M. Cencini, A. Lanotte, and F. Toschi, J. Fluid Mech. **646**, 527 (2010).
[26] K. Gustavsson and B. Mehlig, Phys. Rev. E **84**, 045304 (2011).
[27] J. Salazar and L. Collins, J. Fluid Mech. **696**, 45 (2012).
[28] G. P. Bewley, E. W. Saw, and E. Bodenschatz, New J. Phys. **15**, 083051 (2013).
[29] K. Gustavsson and B. Mehlig, Journal of Turbulence, in press (2014).
[30] K. Gustavsson and B. Mehlig, Phys. Rev. E **87**, 023016 (2013).
[31] K. Gustavsson, J. Einarsson, and B. Mehlig, Phys. Rev. Lett., in press (2014).
[32] J. Sommerer and E. Ott, Science **259**, 334 (1993).
[33] M. Wilkinson and B. Mehlig, Phys. Rev. E **68**, 040101(R) (2003).
[34] B. Mehlig and M. Wilkinson, Phys. Rev. Lett. **92**, 250602 (2004).
[35] J. Kaplan and J. A. Yorke, Springer Lecture Notes in Mathematics **730**, 204 (1979).
[36] M. Wilkinson, B. Mehlig, and K. Gustavsson, Europhys. Lett. **89**, 50002 (2010).
[37] B. J. Devenish, P. Bartello, J.-L. Brenguier, L. R. Collins, W. W. Grabowski, R. H. A. IJzermans, S. P. Malinowski, M. W. Reeks, J. C. Vassilicos, L.-P. Wang, et al., Q. J. R. Meteorol. Soc. **138**, 1401 (2012).
[38] R. A. Shaw, Annu. Rev. Fluid Mech. **35**, 183 (2003).
[39] P. R. Jonas, Atmos. Res. **40**, 283 (1996).